Journal of Molecular Structure 1294 (2023) 136441

Contents lists available at ScienceDirect

Journal of Molecular Structure

journal homepage: www.elsevier.com/locate/molstr

Close-packed small nanocubes assemblies as efficient SERS substrates

P. Varasteanu [a,1], A.M. Bujor [a,b,1], C. Pachiu [a], G. Craciun [a], I. Mihalache [a], V. Tucureanu [a], C. Romanitan [a], R. Pascu [a], A. Boldeiu [a,*]

[a] National Institute for Research and Development in Microtechnologies (IMT-Bucharest), 126A Erou Iancu Nicolae Street, 077190, Voluntari, Romania
[b] Faculty of Chemistry, University of Bucharest, 4-12, Blv. Regina Elisabeta, 030018, Bucharest, Romania

ARTICLE INFO

Keywords:
Close-packed nanocubes assemblies
SERS
Rhodamine 6G
SERS enhancement factor

ABSTRACT

Silver-based nanostructures, especially the anisotropic ones such as triangular nanoplates, nanorods, nanocubes or silver nanowires, are used as Surface enhanced Raman scattering substrates for different analytes sensing, with outstanding results, in terms of the limit of detection (LOD), as well as the enhancement factor (EF), being applicable for early clinical diagnosis of cancer, trace level detection of different organic pollutants, or for the pesticides' detection, and even explosives. Among all these shapes, cubes like nanoparticles (AgNCs) can generate intense hot-spots due to their corners and edges, due to some additional plasmonic modes that occur at different resonance wavelengths in the spectrum, thus, improving SERS sensitivity.

In this work we have successfully synthesized silver AgNCs of 60 nm, that were then assembled on a planar silicon substrate, and use it as a simple SERS substrate towards Rh6G dye. We were able to obtain an averaged calculated EF of 1.78×10^8, with a limit of detection of 4.16×10^{-12} M. Furthermore, the effect of nanocubes' configurations was investigated through the numerical calculations, being revealed that the edge-to-edge arrangement exhibits the highest EF of about 10^9, followed by the edge-to-face (8.6×10^8) and face-to-face (9×10^7) arrangements, in good agreement with experimental calculated value, $\sim 10^8$, considering the frequency of appearance of each configuration.

Our studies related to the use of assemblies of smaller AgNCs on planar silicon surface, with no further nanostructuration process, as SERS based substrates towards one of the most known analyte molecules, as well as an organic dye pollutant, are very encouraging, giving the chance to explore the emerging properties of small nanocubes towards low concentration detection of different organic molecules, thus showing great applicability in both scientific research and practical application, like water pollutants or even foodborne pathogen detection.

1. Introduction

From the industrial revolution, in the last century, a lot of chemicals were released in the Earth atmosphere or in either surface or ground water reserves [1]. Therefore, waters are becoming one of the most suffering systems due to the pollutions, and, in this regard, the organic dyes are important chemicals affecting its quality, since more than 100, 000 synthetic organic dyes types are available commercially worldwide [2,3]. Moreover, these are released from different fields, like textile and fashion industry, painting or food industry, coloring the water and reducing the sunlight penetration, thus affecting the photosynthesis, and subsequently, the aquatic ecosystem or are harmful for humans [4]. The classical analytical tools to detect these pollutants, are generally based on spectroscopic techniques [5–7], which are not focused on in situ detection, so, the need for solutions to develop reliable, low-cost and 'on-site' detection tools become more urgent [8].

Ever since the discovery, in the 1970s, of the Raman enhancement effect [9], Surface Enhanced Raman Spectroscopy (SERS) has become a powerful, nondestructive analytical tool, with high selectivity and sensitivity [10], being able to detect different chemical species through the vibrational fingerprints. During last years, this was extensively used to identify a wide range of molecules, which are affecting various fields, such as human health [11], environmental pollutants [12–14], pesticides [15,16], food safety [17] and even explosives [18,19]. As stated before, the electromagnetic enhancement is playing the leading role, due to the localized surface plasmon resonance (LSPR) excitation of the metallic nanostructures, when the so-called '*hot spots*' are forming [20–22]. Therefore, tremendous efforts have been made to prepare

* Corresponding author.
E-mail address: Adina.boldeiu@imt.ro (A. Boldeiu).
[1] These authors contributed equally to this work.

https://doi.org/10.1016/j.molstruc.2023.136441
Received 1 June 2023; Received in revised form 28 July 2023; Accepted 16 August 2023
Available online 18 August 2023

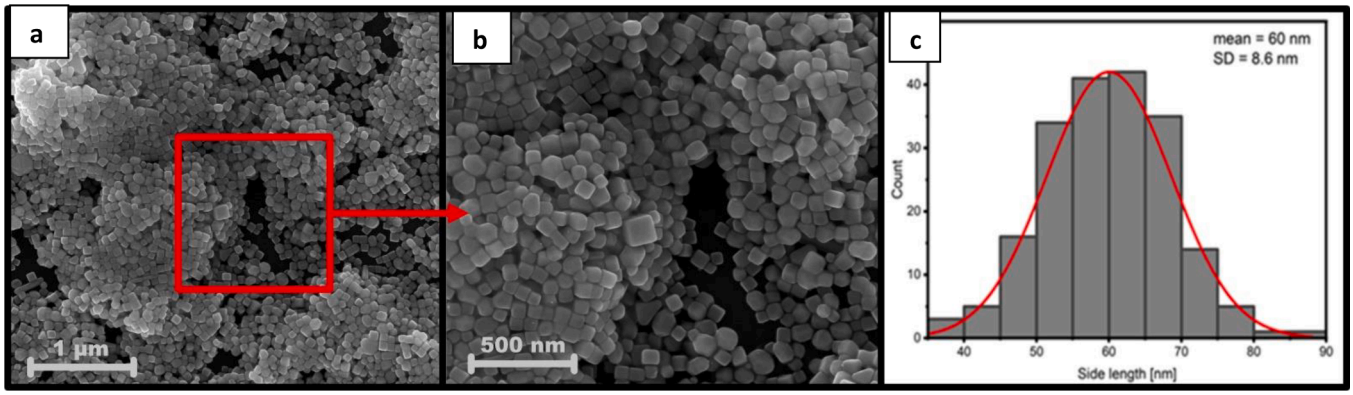

Fig. 1. (a, b) SEM micrographs of the synthesized AgNCs; (c) The histogram of the nanocubes dimensions.

highly ordered plasmonic metallic nanostructures or assembly of plasmonic nanomaterials [23]. Due to its remarkable enhancement effect that has been revealed [24], Ag-based nanostructures with different morphologies, like nanospheres [25,26], triangular nanoplates [27], nanorods [28], nanocubes or Ag nanowires [29,30] and nanodecahedra [31] were used as SERS substrates for different analytes sensing. Compare to spheres like nanoparticles, a strong enhancement of the electromagnetic field was observed in the case of the anisotropic morphologies, due to their shapes, like corners, edges or tips [32]. Among all these shapes, cubes like nanoparticles (AgNCs) can generate intense hot-spots due to their corners and edges, due to some additional plasmonic modes that occur at different resonance wavelengths in the spectrum, thus, improving SERS sensitivity [33,34]. Their use as highly sensitive SERS substrates can have outstanding results, in terms of the limit of detection (LOD), as well as the enhancement factor (EF), being applicable for early clinical diagnosis of cancer [35], trace level detection of different organic pollutants [36], or for the pesticides' detection [16], and even explosives [37,38]. In this regard, the enhancement factors of SERS show strong sensitivity between the nanoparticle size and shape [39].

Rhodamine 6 G is an organic chloride salt and a xanthene dye, a dark red powder, water soluble, non-volatile, very popular as model analyte to probe SERS enhancement of different substrates and a fluorescence marker, as well. It is one of the toxic dyes, used as a colorant in the textile industries, and water containing rhodamine dyes causes irritation of the skin, eyes and respiratory system of human beings. It was also stated that drinking water contaminated with rhodamine dyes is highly carcinogenic and poisonous to living organisms [40]. There were some studies about rhodamine detection using silver nanocubes decorated GO nanosheets on different types of support, as SERS substrate. In this regard, AgNCs of 120 nm in edge length mixed with GO nanosheets were used as free-standing hybrid paper for SERS detection of rhodamine, with a low detection limit of 10^{-10} M [41], or 56 nm Ag@SiO_2 NCs assembled on modified nano-paper was used as an active SERS substrate with an EF of 1.49×10^7 towards rhodamine [42]. GO@AgNPs based pyramid silicon based flexible structure was used as SERS substrate, the EF reaching up to 8.1×10^9 using rhodamine 6 G as the probe molecule [43]. Ag nanocubes with sizes of 40, 60 and 80 nm were used to investigate the SERS performances using crystal violet (CV) molecules as analyte [39].

Looking back to the reports related to the use of smaller AgNCs as SERS substrates towards rhodamine dye detection, we observed only a few studies. So, in this paper, we have synthesized silver nanocubess having the mean edge length of 60 nm, that were then assembled on a planar silicon substrate, and use it as a simple SERS substrate towards Rh6G dye. We were able to obtain an averaged calculated EF 1.78×10^8, with a limit of detection of 4.16×10^{-12} M. Furthermore, the effect of nanocubes' configurations was investigated through numerical calculations, being revealed that the edge-to-edge arrangement exhibits the highest EF of about 10^9, followed by the edge-to-face (8.6×10^8) and face-to-face (9×10^7) arrangements, in good agreement with experimental calculated value, $\sim 10^8$, considering the frequency of appearance of each configuration.

2. Experimental

2.1. Materials

All the chemicals used for our synthesis were purchased from different suppliers, and further used without any purification. Silver trifluoroacetate (CF_3COOAg) was purchased from Alfa Aesar, ethylene glycol (EG) from Honeywell, while sodium hydride (NaHS), Rhodamine (Rh6G), and hydrochloric acid (HCl) were all from Sigma-Aldrich. Polyvinylpyrrolidone (PVP), average mol. wt 40,000 (PVP K40) was supplied from ChemCruz. High-purity water from Carl Roth was used in all experiments. Prior to use, all glassware was washed for 20 min in aqua regia (volume ratio HCl/HNO_3 = 3/1), followed by rinsing with deionized water and drying under a nitrogen stream.

2.2. Methods

The FESEM images were obtained with a Field Emission Scanning Electron Microscope from NOVA NanoSEM 630 (ThermoFisher Scientific, USA). *UV–vis analysis* was carried out using a U-0080D biospectrophotometer from Hitachi High Technologies. *Infrared spectra* of the prepared nanostructures were recorded in the region of 400–4500 cm^{-1} on a FTIR Vertex 80 V (Bruker Optics, USA), under transmittance mode operating at 2 cm^{-1} wave number resolution. X-ray diffraction pattern was performed on Rigaku X-ray diffraction, Japan, using Cu K_α radiation source, with a scan rate of 8 deg. m^{-1} and recorded in 2θ range, from 20 to 80°. Dynamic light scattering (DLS) and electrophoretic light scattering (ELS) were used to measure the hydrodynamic diameters and surface charge of the obtained nanocrystals, using Beckman Coulter (USA) Delsa™Nano C instrument. A laser diode of 658 nm illuminated the nanoparticles, producing time-dependent fluctuations in the intensity of laser light, while the angle for size measurements is 165° and 15° for z-potential measurements. The measurements were performed at 25°C. For data analysis, each sample measurement was performed in triplicate and the DelsaNano 3.73/2.30 software was used to further process the data.

The Raman spectra and all the SERS measurements were recorded at room temperature with a Witec Raman spectrometer (Alpha-SNOM 300 S, WiTec. GmbH, Ulm, Germany) using 532 nm as an excitation and a maximum power of 145 mW. The incident laser beam with a spot-size of ~ 1.0 µm was focused with a 50 × objective, and 10 s the exposure time and 3 accumulations.

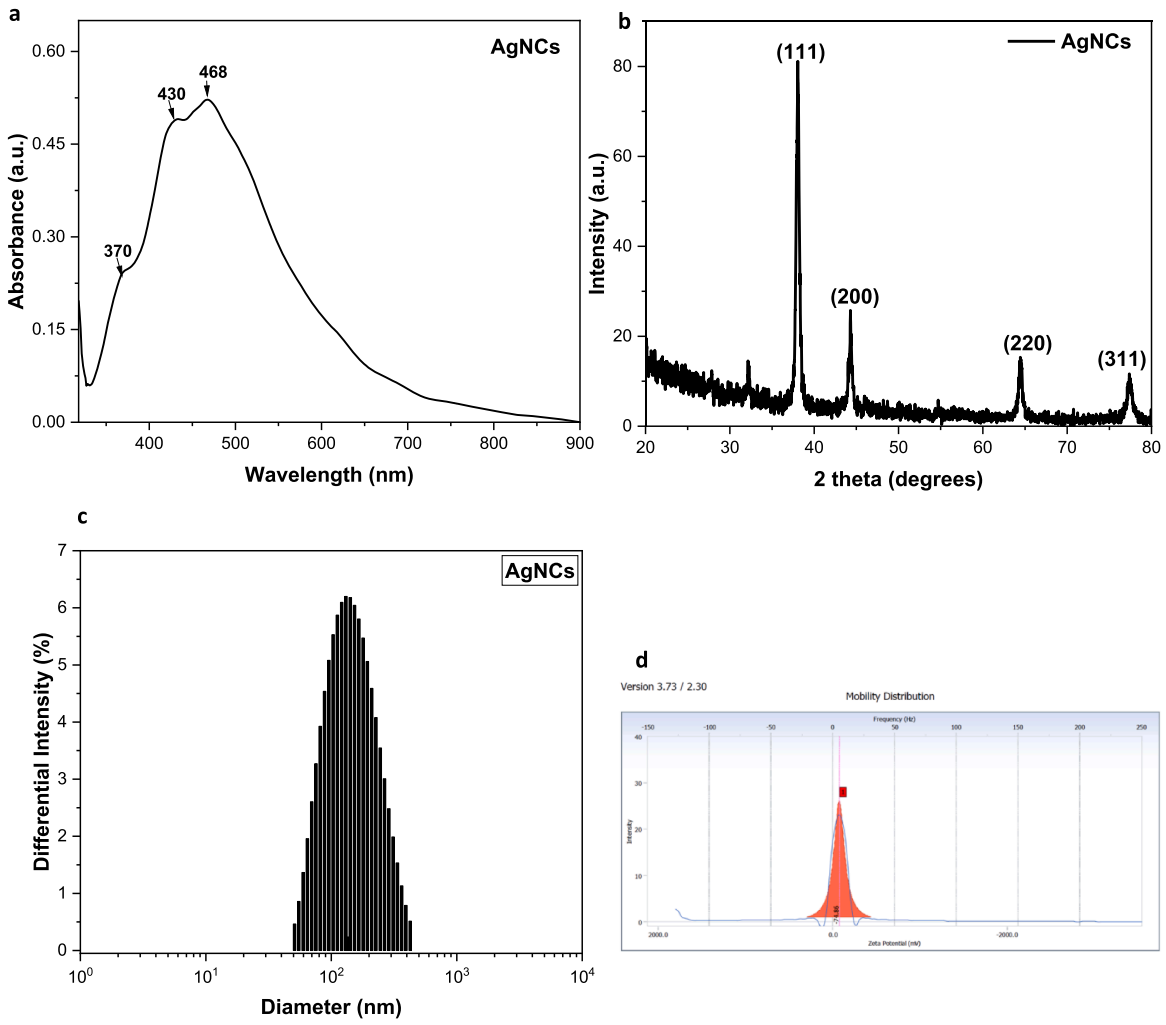

Fig. 2. (a) UV spectra of the synthesized AgNCs. The histogram of the nanocubes dimensions;(b) XRD pattern; (c) DLS measurements of the AgNCs; (d) zeta potential value.

2.3. Silver nanocubes synthesis

Before synthesis, all the glasswares were washed with fresh aqua regia and washed several times with ultrapure water. We have applied an adjusted polyol method, reported by Zhang et al.' protocol [44], using very small volumes of sulfide sodium hydride and hydrochloric acid to obtain the silver nanocubes. The small volumes of NaSH decrease over all the reaction time, while the chloride ions assure an oxidative etching media, both of them improving the quality and reproducibility of the synthesis method. Specifically, 5 mL of EG were added into a glass round bottom flask and heated at 150 °C, for one hour, under magnetic stirring. Then, 60 μL of NaSH 3 mM were added, followed by the addition of 500 μL HCl 3 mM. The PVP was then injected into the heated solution, by adding 1250 μL of 180 mM (monomer concentration). Finally, 400 μL of CF_3COOAg 141 mM were added. The reaction was stopped by placing the flask in ice-water bath to cool down. After cooling down, the colloidal solution was centrifuged with acetone and ethanol, at 8500 RPM, for 20 min, in order to eliminate the PVP excess and ethylene glycol. Finally, the prepared AgNCs were dispersed in ethanol, and kept in dark conditions.

3. Results and discussions

3.1. Characterization of the AgNCs

The obtained plasmonic nanostructures were firstly characterized by *SEM microscopy* in order to investigate their morphology, the results being revealed in Fig. 1. In this regard, the silicon Si (100) substrates (1 cm × 1 cm) were firstly cleaned in Piranha solution (a mixture of sulfuric acid (>96%) and hydrogen peroxide (31%) in 3:1 vol ratio), followed by rinsing in isopropyl alcohol, and deionized water for several times, and dried under the nitrogen flow, and used as substrate for SEM investigations. The micrographs shown in Fig. 1 (a, b), reveal agglomerated nanocubes, having the mean edge lengths of 60 ± 8 nm, according to the plotted histogram, the corresponding sharp corners and edges being also highlighted.

The *UV–Vis* analysis shows in Fig. 2(a) a broad SPR band, having the absorption maximum around 468 nm, along with two shoulders peaks observed at 370 and 430 nm, revealing the dependence between size of the nanocubes and their absorption spectra [45]. The X ray pattern (Fig. 2(b)) reveals the main peaks of 2θ values at 38.06°, 44.25°, 64.40° and 77.37°, corresponding to Ag (111), (200), (220) and (311) planes of cubic silver, which is in good agreement with the Joint Committee on Powder Diffraction Standards (JCPDS file No. 04–0783), and in agreement with the literature [46]. The DLS measurements shown in Fig. 2(c) reveal a narrow distribution of the hydrodynamic diameter, with the

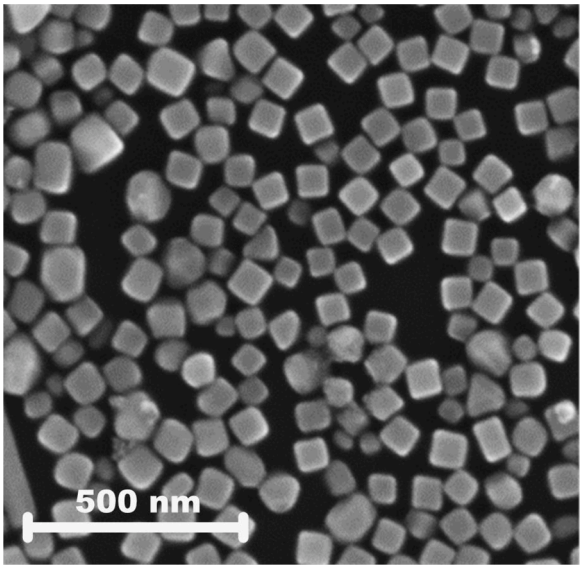

Fig. 3. SEM image of the AgNCs after dodecanethiol addition, resulting in a close-packed arrangement, like edge-to-edge, face-to-face, edge-to-face.

mean diameter of 120 nm, with a polydispersity index of 0.134, indicating the monodispersed nanocubes solution that we obtained. Additionally, the measured zeta potential was −74.86 mV, suggesting the solution stability.

3.2. SERS substrates fabrication, characterization and performance analysis

In order to study the interaction between our prepared 60 nm Ag nanocubes and the Rh6G, we deposited the metallic nanostructures on clean silicon substrates, previously described.

The SERS substrates were built by drop-casting volumes of 50 µl AgNCs on planar silicon support following the addition of 10 µl mixture solution containing 1-dodecanethiol and ethanol, 1:5 vol ratio. This step allowed the nanocubes to be arranged into some close-packed structures with certain configurations, like edge-to-edge, edge-to-face, face-to-face, as presented in Fig. 3.

After almost 30 min, 50 µl of Rh6G aqueous solutions with concentrations ranging from 10^{-9} to 10^{-13} M were dropped and left to interact for 2 h, on the shaker, at 250 RPM, in darkness, to improve the arrangement and to speed up solvent evaporation. These concentrations were sequential dilutions from the standard stock solution of 10^{-3} M Rhodamine 6 G in deionized water.

The IR spectroscopy was used to study the interaction between the silver nanocubes and the chosen probe molecule.

Regarding the IR spectroscopy evaluation, in Fig. 4a, the spectra of pure PVP and AgNCs were shown. In the case of PVP spectra, there are two strong peaks at 1647 and 1287 cm^{-1}, assigned to the stretching vibration of C=O and C—N stretching bonds [47], respectively, while the bending vibration of this latter bond are located at 1014 and 1068 cm^{-1}. After the nanocubes synthesis, these two peaks are shifted towards higher wavenumbers, at 1050 and 1106 cm^{-1}, indicating a stronger coordination between the pyrrolyl nitrogen electrons to the Ag atoms [48]. At the same time, the peak located at 1647 cm^{-1} is shifted to 1681 cm^{-1}, maybe due to an intense interaction during the chemical

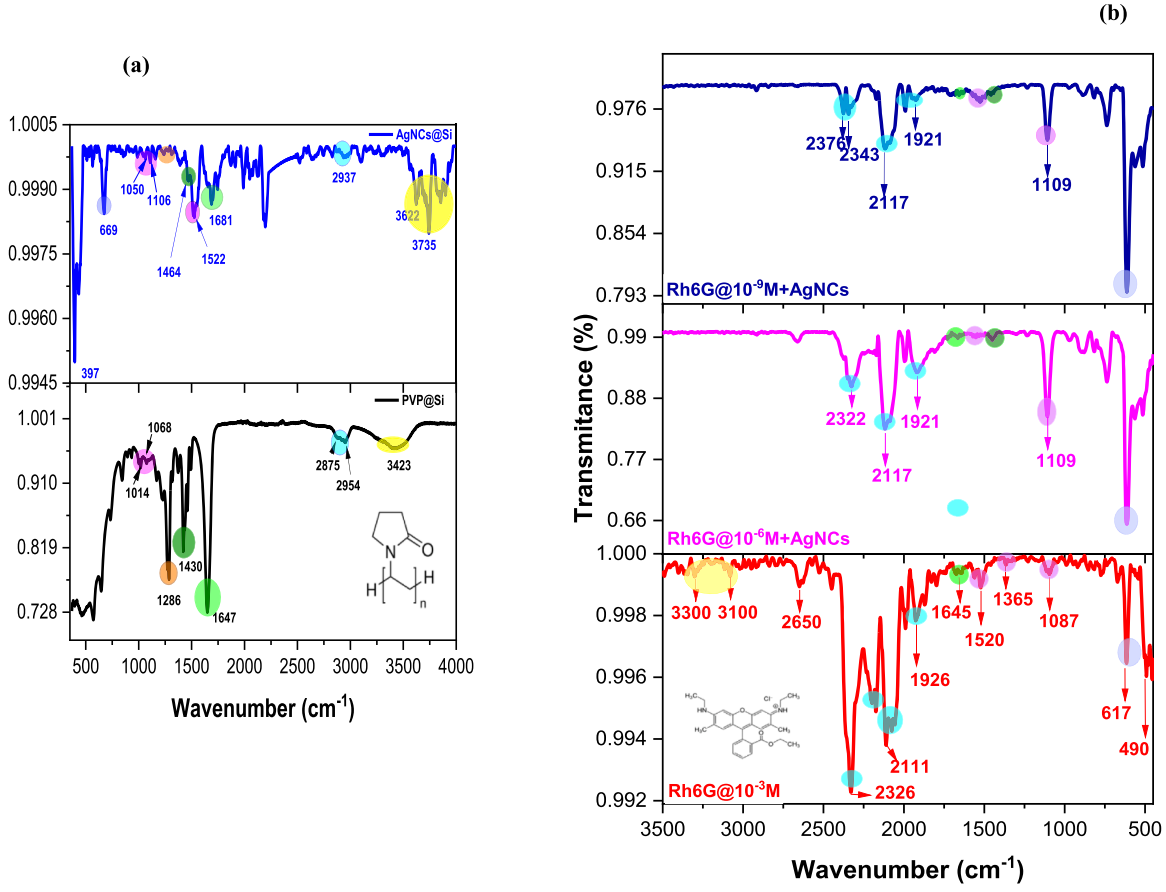

Fig. 4. (a) FT-IR analysis of the synthesized AgNCs and of PVP; (b) FT-IR analysis of Rh6G@10⁻3 M and its interaction with AgNCs at different concentrations Rh6G@10^{-6}M+AgNCs and Rh6G@10^{-9}M+AgNCs. Insets in (a) show the PVP structure, and in (b), the Rh6 structure.

Table 1
FT-IR, Raman and SERS peaks assignments for Rh6G and Rh6G+AgNCs.

FT-IR of Rh6G (cm^{-1})	Raman of Rh6G (cm^{-1})	SERS of Rh6G 10^{-6}M+AgNCs (cm^{-1})	Peak assignments
–	–	**238**	Ag-O bond
490	–	–	Si-O vibrations
–	**522**	**522**	Si peak
617	**608**	**608**	C-C-C ring in plane bending/ C-S stretching from thiol
670	–	–	Cl^-anion
–	–	**707/1075**	C-S stretching
737	**778**	**778**	C—H out of plane bending
921	–	**926**	-CH_2 stretching
1095	–	**1095**	COO^- stretching
	1177	**1126**	C-H out of /in plane vibration
–	**1257**	**1257**	C–O–C stretching
–	–	**1307**	N-H in plane
1365	**1345/ 1428**	**1361/1440**	aromatic C—C/C—N stretching
1520	**1530**	**1545**	aromatic C-C stretching
1560	**1595**	**1570**	xanthene ring stretching / N-H in plane
1645	**1646**	**1646**	aromatic C=C stretching of the Rh6G skeleton

process, and further, a possible coordination to Ag atom from the nanocubes [49], strengthened by the band from 1522 cm^{-1}] attributed to the N-Ag coordination [39].

The strong peak from 1430 cm^{-1} assigned to tertiary nitrogen vibration in the case of PVP spectra is still visible after the synthesis, being shifted to 1464 cm^{-1}. Additionally, the peak from 669 cm^{-1} is given by the C—C vibrations in the ring [6], while the intense and broad peak around 397 cm^{-1} might correspond to the silver metal [50]. Moreover, the C—H vibrations bonds are revealed in both cases, PVP and AgNCs, by the bands around 2875 cm^{-1} and 2937 cm^{-1}, while the presence of hydroxils is marked by the broad band from 3423 cm^{-1}.

Accordingly, in Fig. 4b are revealed the IR spectra for Rh6G as well as for the its interactions with the prepared silver nanocubes, at 10^{-6} and 10^{-9} M, respectively, with an inset representing the molecular structure of Rh6G. For the Rhodamine 6 G spectra, the bands absorption from 3300 and 3100 cm^{-1} are due to the N—H bond stretching [51]. The high number of small peaks in the region 3100–2650 cm^{-1}, as well as the intense bands between 2326 and 1921 cm^{-1} from the IR spectra of Rh6G, as well as the ones from 1560 and 1365 cm^{-1}, could be ascribed to the xanthene ring from its structure [52]. Chlorine ion from rhodamine solution is revealed by the peak from 670 cm^{-1}, while the one from 490 cm^{-1} could be assigned to the Si-O vibrations from the substrate [53].

After the interaction with the silver nanostructures, some of these peaks are disappearing (e.g. 1645, 1520 cm^{-1}), or shifted (the one from 1095 to 1107 cm^{-1}, attributed to stretching vibration of COO^-), and even, there are observed some new ones, e.g. the absorption band from 1440 cm^{-1} assigned to the CH_3N stretching mode. The low band from 737 cm^{-1} shown in Rh6G spectra, assigned to the di-substituted aromatic ring is increased after the interaction between the probe molecule and AgNCs [54]. Detailed bands assignment is presented in Table 1.

An important characteristic is the fact that by decreasing the Rh6G concentration when reacting with Ag-based nanostructures, the intensity of the bands is also decreasing.

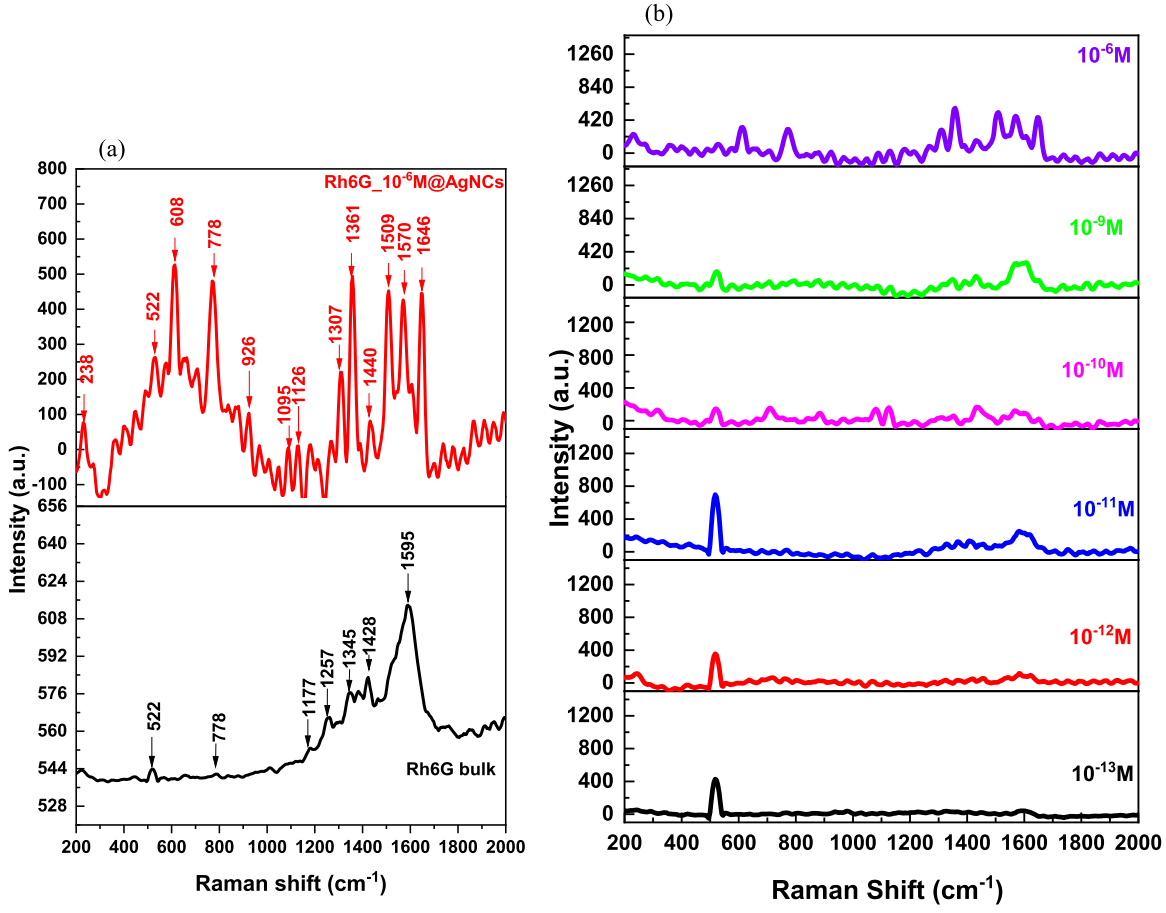

Fig. 5. (a) Raman and SERS spectra of Rh6G bulk and of Rh6G 10^{-6} M on AgNCs-based substrate; (b) SERS spectra of probe molecule on AgNCs, at different Rh6G concentrations. All spectra were subjected to baseline substraction.

Table 2
Calculated EF for the selected bands.

Analyte molecule	Signals (cm^{-1})	Calculated EF
Rh6G	608	**1.08×10^8**
	1257	**2.06×10^8**
	1361	**2.04×10^8**
	1646	**1.96×10^8**

Next, there were recorded the Raman and SERS spectra corresponding to Rhodamine 6 G powder (namely as Rh6G bulk) and AgNCs@Rh6G_10^{-}6 M, and shown in Fig. 5a. First, we recorded Raman spectra of Rh6G on clean Si substrate, and there were not observed the all the distinct Raman peaks. When using silver nanocubes as a substrate, all the characteristic bands of the xanthene ring are revealed for the probe molecule, as follows: 608, 778 and 1126 cm^{-1} (C—C-C ring bending, C—H out of /in plane vibration), 1307 and 1570 cm^{-1} (N—H in plane vibration), 1361/1440/1545 cm^{-1} (aromatic C—C/C—N stretching mode) [55]. Additionally, the peak from 520 cm^{-1} could be attributed to the Si from the substrate [56], which is increasing by decreasing the rhodamine concentration, while the ones from 926 and 238 cm^{-1} are assigned to the PVP Raman modes, used for the nanocubes synthesis [57], and the stretching vibration of C-S bond as result of dodecanthiol adsorption of silver nanocubes surface [58], respectively. This is sustained by the two peaks from 707 and 1075 cm^{-1}, also assigned to the stretching C-S bond from the thiol onto silver surface. Moreover, the aromatic stretching vibration from 1646 cm^{-1} could be assigned to the Rh6G molecule adsorption on the nanocubes surface, as indicated elsewhere [59,60].

The efficiency of our silver-based SERS substrate was further evaluated, by recording the SERS spectra of Rh6G with concentrations ranging from 10^{-}9 M to 10^{-13}M on the AgNCs, as depicted in Fig. 5b. There are observed most of the prominent peaks of the Rh6G previously reported, and by going down to lower concentrations till 10^{-13}M, their intensities are also decreasing. The presence of chlorine ion from rhodamine solution is revealed by the peak from 670 cm^{-1}. The bands assignment is summarized in Table 1.

Going further, the performance of the prepared substrate was investigated, and the calculated EF values of the Rh6G molecule adsorbed on 60 nm AgNCs based substrate, for the most significant bands are listed in the *Table 2*:

The formula used to calculate the EF for the Rh6G, when using our prepared silver nanocubes-based substrate is given below [30]:

$$EF = I_{SERS} \times N_{bulk}/I_{RS} \times N_{SERS} \quad (1)$$

where I_{SERS} and I_{RS} represent the intensity of the band in SERS and Raman spectra respectively, N_{bulk} is the number of molecules that probed the Raman measurement sample, N_{SERS} is the number of rhodamine molecules probed in SERS.

The Rh6G molecules' number was estimated using the formula [30],

$$N_{SERS} = CVN_A S_{scan}/S_{sub} \quad (2)$$

$$N_{bulk=}M\rho hN_A A_{Raman} \quad (3)$$

where C = molar concentration of Rh6G (10^{-}6 M), V = droplet 'volume (50 μL), N_A= Avogadro number (6.023×10^{23}), S_{scan} = area of Raman scanning, S_{sub} = area of the substrate, M and ρ represent molecular weight and density of Rh6G, respectively, (M = 479.02 u.a.m., ρ = 1.26 g/cm^3), h is the confocal depth, and A_{Raman} = laser spot diameter (1.62 μm, calculated for 532 nm laser wavelength).

$$A_{Raman} = 1.22 \times \lambda/NA \quad (4)$$

where, λ=532 nm and NA =0.4; $A_{Raman} = 1.62$ μm. For 10^{-}6 M Rh6G, and considering $S_{scan}/S_{sub=}A_{Raman}= 1.62$ μm, we obtained the following values for N_{SERS} and N_{bulk}:

$$N_{SERS} = 48.78 \times 10^6 molecules;$$

$$N_{bulk=}12.37 \times 10^{14} molecules;$$

The Rh6G limit of detection (LOD) was estimated using the values of the 1650 cm^{-1} SERS peak intensities. A near-linear dependence of peaks intensities as a function of Rh6G concentrations, ranging from 10^{-9} to 10^{-13} M, is observed. Hence, a linear fit on this calibration curve is necessary to determine the LOD according to eq. below [61,40]:

$$LOD = 3.3 \times SD/slope \quad (5)$$

where *SD* is standard deviation, and *the slope* of the calibration curve.

Finally, our obtained value was 4.16×10^{-12} M. This value, as well as the one for EF (1.78×10^8)

These values could be the result of the Ag nanocubes uniform distribution on the silicon substrate, which created a very small space between them, creating an LSP-SPP (localized surface plasmon of AgNCs – surface plasmon polariton) coupling effect, generating thus, the hot spots. Additionally, the reported EF or limit of detection corresponding to the Rh6G detection using AgNCs-based SERS substrates were gathered and listed in Table 3.

The EF that we obtained is comparable to that from roughened Au film (2.5×10^8) or from micro-ring arrays of silver (Ag) nanostructures (8.85×10^8), as reported in the literature [40,62], when talking about Rh6G detection.

A very important remark is that low detection limits or high EFs were recorded when using silver nanocubes in different hybrid nanostructures, like GO, or using different support, as gold, glass or nanostructurated silicon. Overall, it seems to be very encouraging using this type of SERS substrate for further sensing investigations.

Table 3
Summary of literature survey for Rh6G detection by AgNCs-based SERS substrate.

SERS substrate type	Laser (nm)	Analyte molecule	EF	Limit of detection [M]	Reference
AgNCs of 500 nm on Si substrate	785	RhB	10 [7]	10^{-15}	[21]
AgNCs of 60, 90, 115 nm on PE@Au film substrate	633	Rh6G	–	10^{-10}	[33]
AgNCs of 106 nm on Si substrate	514	Rh6G	4.5×10^6	–	[34]
106 nm AgNCs on Au substrate	514	Rh6G	2.3×10^8	–	
153 nm AgNCs on glass substrate	633	Rh6G	8.71×10^{10}	–	[38]
80 nm Ag nanocubes	532	CV	3.1×10^5	–	[39]
120 nm AgNCs@GO hybrid paper substrates	532	Rh6G	–	10^{-10}	[40]
SiO2@AgNCs of 56 nm on Fe-TiO_2 NS paper	633	Rh6G	1.49×10^7	–	[41]
GO@AgNPs based pyramid silicon		Rh6G	8.1×10^9	–	[43]
Ag nanotriangles@259 nm	532	Rh6G	6.8×10^7	10^{-11}	[46]
roughened Au film	532	Rh6G	2.5×10^8	7.1×10^{-11}	[40]
micro-ring arrays of Ag nanostructures	532	Rh6G	8.85×10^8	–	[62]
AgNCs@60nm	**532**	**Rh6G**	**1.11×10^8**	**4.16×10^{-12}**	**our work**

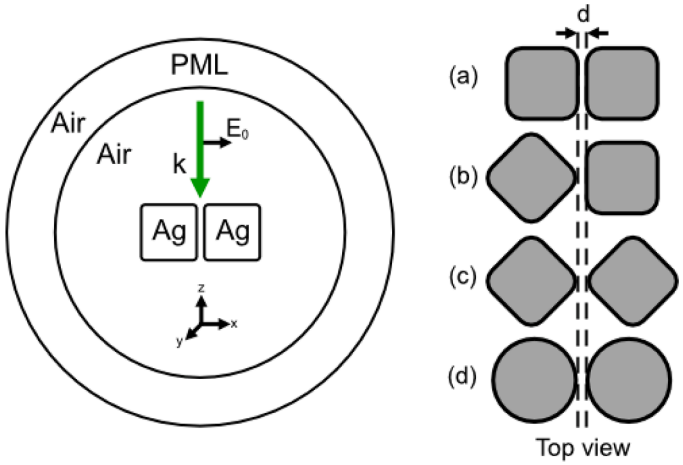

Fig. 6. Left-hand side, a schematic illustration of simulated domain, and on the Right-hand side, a top view schematic of each proposed arrangements of particles on the substrate: (a) face-to-face, (b) edge-to-face, (c) edge-to-edge, and (d) nanospheres used for reference.

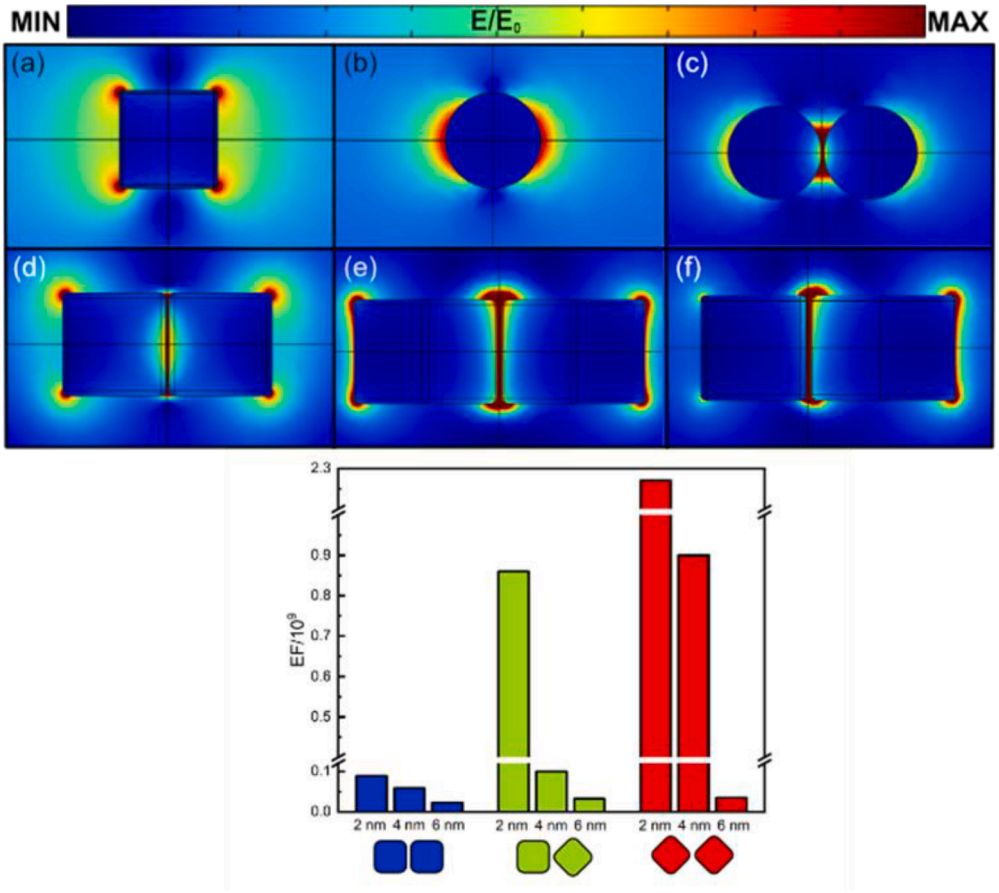

Fig. 7. Top: Electromagnetic field distribution for each proposed particles configuration: (a) single cube with the edge length of 60 nm. (b) single sphere (used for reference) with a diameter of 60 nm, and from (c) to (f) the proposed configurations in front view for clarity; Bottom: Variation of EFs for different interparticle distances (2, 4, 6 nm) for the three considered configurations.

3.3. Numerical analysis

In order to validate the SERS enhancement factor obtained by Raman spectroscopy studies, a series of Finite Element Method (FEM) simulations in COMSOL Multiphysics® [63] were performed. By analyzing the SEM micrograph in Fig. 3, a few AgNCs configurations could be found, such as: face-to-face, edge-to-face and edge-to-edge. These configurations together with the simulation domain are illustrated in Fig. 6a.

The electromagnetic enhancement factor (EF) was calculated by employing the Scattered Field Formulation in Comsol's Wave Optics module, using the following formula: $|\frac{E}{E_0}|^4$, where E is the maximum electric field in the presence of the particles, whereas E_0 (background field) is the incidence electric field (without any particles). The refractive indices of silver (Ag) at a wavelength of 530 nm (excitation wavelength in our study), were taken from literature [64].

It is important to mention that Perfectly Matched Layers were used to absorb all the unwanted reflections from the system. A linear polarized plane wave was used to excite the system, the incidence wave's electric field amplitude being considered arbitrary as 1 V/m. The edge length of AgNCs was 60 nm as the mean value obtained from ImageJ analysis of SEM micrographs. The vertices were rounded to avoid the lighting rod effects and numerical instabilities (where the electric field tends to infinity) and the radius of curvature was set as 2 nm. In addition to the aforementioned configurations, where the distance between the particles was considered 2 nm, two additional inter particle distances (4 nm and 6 nm) were considered in order to have a complete picture of the whole system and also to take into account the stochasticity of particles arrangements on the substrate.

The AgNCs systems were compared with the spherical nanoparticles of 60 nm in diameter (the same as the edge length) considering the same spacing between them, since it was revealed that the nanocubes'enhancement is greater compared to the spheres like nanoparticles with the same size thanks to more efficient separation of charges and high curvature corners present in the NCs that allow accumulation for larger charge.

The electromagnetic field for each configuration is illustrated in Fig 7, where it can be seen that the electric field in the case of the single nanocube is located at the vertices (Fig. 7a), in comparison with the nanosphere, where the field is concentrated on the particle surface (Fig. 7b). When two particles are considered, as in Fig. 7c–f, and placed very close to each other ($d = 2$ nm), the electric field is more confined in the space between them than at their extremities.

The highest EF- 10^9, was obtained for the edge-to-edge configuration (Fig. 7e), while the lowest one was exhibited by the nanosphere's configuration, 6×10^7, very close to the one for the face-to-face case, 9×10^7 (Fig. 7d). This could be in accordance with the results obtained by Rabin and Lee that claims that the face-to-face assemblies of the nanocubes give a decreased enhancement, while the edge-to-edge might be responsible for the highest enhancement [65]. Going further, in the case of edge-to-face arrangement, the EF was 8.6×10^8 and, when the distance between particles is increased to 6 nm, the EF's decreases to 2×10^5 for the nanosphere configuration.

Therefore, given the weight each particles arrangements on the surface throughout the area scanned by the laser, an experimental calculated electromagnetic EF of about 10^8 it is attainable for AgNCs with a mean side length of 60 nm.

4. Conclusions

In this work we successfully synthesized silver nanocubes having the mean edge length of 60 nm, which were then analyzed by electronic microscopy, X-ray diffraction, as well as several, spectroscopies techniques, such as UV, FT-IR and DLS.

Going further, simple, efficient and low-cost SERS substrate based on these anisotropic nanostructures was prepared on planar silicon support, and using it towards rhodamine 6 G dye. The obtained close-packed structures provided highly sensitive detection of Rh6G up to 10^{-13}M, and the calculated limit of detection was 4.16×10^{-12} M, while the averaged calculated EF was of 1.78×10^8. In addition, the effect of nanocubes' arrangement was probed through the theoretical calculations, being reported that the edge-to-edge arrangement exhibits the highest EF of about 10^9, followed by the edge-to-face (8.6×10^8) and face-to-face (9×10^7) arrangements, in good agreement with experimental calculated value, ~10^8, considering the frequency of appearance of each configuration.

Our studies related to the use of assemblies of smaller AgNCs on planar silicon surface, with no further nanostructuration process, as SERS based substrates towards one of the most known analyte molecules, as well as an organic dye pollutant, are very encouraging, giving the chance to explore the emerging properties of small nanocubes towards low concentration detection of different organic molecules, thus showing great applicability in both scientific research and practical application, like water pollutants or even foodborne pathogen detection.

Declaration of Competing Interest

The authors declare that they have no known competing financial interests or personal relationships that could have appeared to influence the work reported in this paper.

Data availability

Data will be made available on request.

Acknowledgments

Many thanks to Oana Brancoveanu for additional SEM characterization.

This work was supported by a grant of the Ministry of Research, Innovation and Digitization, CNCS - UEFISCDI, project number PN-III-P1-1.1- TE-2021-1357, within PNCDI III.

References

[1] A. Nazir, P. Huo, H. Wang, Z. Weiqiang, Y. Wan, A review on plasmonic-based heterojunction photocatalysts for degradation of organic pollutants in wastewater, J. Mater. Sci. 58 (15) (2023) 6474–6515, https://doi.org/10.1007/s10853-023-08391-w.

[2] U. Shanker, M. Rani, V. Jassal, Degradation of hazardous organic dyes in water by nanomaterials, Environ. Chem. Lett. 15 (2017) 623–642, https://doi.org/10.1007/s10311-017-0650-2.

[3] Y. Yang, J. Li, J. Luo, Y. Ding, P. Song, Effect of surface hydroxyls and porous nanostructured sensors integrated for SERS monitoring and efficient removal of organic pollutants, Appl. Surf. Sci. 601 (2022), 154123, https://doi.org/10.1016/j.apsusc.2022.154123.

[4] S. Hussain, et al., Contamination of Water Resources by Food Dyes and Its Removal Technologies. Water Chemistry 05, IntechOpen, 2020, https://doi.org/10.5772/intechopen.90331.

[5] E.M. Carstea, J. Bridgeman, A. Baker, D.M. Reynolds, Fluorescence spectroscopy for wastewater monitoring: a review, Water Res. 95 (2016) 205–219, https://doi.org/10.1016/j.watres.2016.03.021.

[6] D. De Souza, S.A.S. Machado, Electrochemical detection of the herbicide paraquat in natural water and citric fruit juices using microelectrodes, Anal. Chim. Acta 546 (2005) 85–91, https://doi.org/10.1016/j.aca.2005.05.020.

[7] C. Xu, J. Wang, L. Wan, J. Lin, X. Wang, Microwave-assisted covalent modification of graphene nanosheets with hydroxypropyl-β-cyclodextrin and its electrochemical detection of phenolic organic pollutants, J. Mater. Chem. 21 (2011) 10463–10471, https://doi.org/10.1039/C1JM10478K.

[8] B.O. Asamoah, et al., Towards the development of portable and *in situ* optical devices for detection of micro-and nanoplastics in water: a review on the current status, Polymers (2021), https://doi.org/10.3390/polym13050730.

[9] M. Fleischmann, P.J. Hendra, A.J. McQuillan, Raman spectra of pyridine adsorbed at a silver electrode, Chem. Phys. Lett. 26 (1974) 163–166, https://doi.org/10.1016/0009-2614(74)85388-1.

[10] E.C. Le Ru, P.G. Etchegoin, Single-molecule surface-enhanced Raman spectroscopy, Annu. Rev. Phys. Chem. 63 (2012) 65–87, https://doi.org/10.1146/annurev-physchem-032511-143757.

[11] N.T.T. Phuong, T.X. Hoang, N.L.N. Tran, L.G. Phuc, V.D. Phung, H.K.T. Ta, T. N. Bach, N.H.T. Tran, K.T.L. Trinh, Rapid and sensitive detection of Rhodamine B in food using the plasmonic silver nanocube-based sensor as SERS active substrate, Spectrochim. Acta Part A 263 (2021) 120179–120187, https://doi.org/10.1016/j.saa.2021.120179.

[12] L.R. Terry, S. Sanders, R.H. Potoff, J.W. Kruel, Jain M, H. Guo, Applications of surface-enhanced Raman spectroscopy in environmental detection, Anal. Sci. Adv. 3 (2022) 113–145, https://doi.org/10.1002/ansa.202200003.

[13] G. Bodelón, I. Pastoriza-Santos, Recent progress in surface-enhanced raman scattering for the detection of chemical contaminants in water, Front. Chem. 8 (2020) 478–486.

[14] C. Han, J. Chen, X. Wu, Y.W. Huang, Y. Zhao, Detection of metronidazole and ronidazole from environmental Samples by surface enhanced Raman spectroscopy, Talanta 128 (2014) 293–298, https://doi.org/10.1016/j.talanta.2014.04.083.

[15] A. Bernat, M. Samiwala, J. Albo, X. Jiang, Q. Rao, Challenges in SERS-based pesticide detection and plausible solutions, J. Agric. Food Chem. 67 (45) (2019) 12341–12347, https://doi.org/10.1021/acs.jafc.9b05077.

[16] S. Augustine, K.P. Sooraj, V. Pachchigar, C.M. Krishna, M. Ranjan, SERS based detection of Dichlorvos pesticides using silver nanoparticles arrays: influence of array wavelength/amplitude, Appl. Surf. Sci. 544 (2021) 148878–148886, https://doi.org/10.1016/j.apsusc.2020.148878.

[17] F. Saviñon-Flores, E. Méndez, M. López-Castaños, A. Carabarin-Lima, K.A. López-Castaños, M.A. González-Fuentes, A. Méndez-Albores, Review on SERS-based detection of human virus A. infections: influenza and coronavirus, Biosensors 11 (3) (2021) 66–95, https://doi.org/10.3390/bios11030066.

[18] S. Adhikari, E.K. Ampadu, M. Kim, D. Noh, E. Oh, D. Lee, Detection of explosives by SERS platform using metal nanogap substrates, Sensors 21 (2021) 5567–5575, https://doi.org/10.3390/s21165567.

[19] Y. Huang, W. Liu, Z. Gong, W. Wu, M. Fan, D. Wang, A.G. Brolo, Detection of buried explosives using a surface-enhanced Raman Scattering (SERS) substrate tailored for miniaturized spectrometers, ACS Sens. 5 (9) (2020) 2933–2939, https://doi.org/10.1021/acssensors.0c01412.

[20] M.B. Bhavya, P.B. Ramya, M.S. Bhamy, S. Maithry, B. Prangya, S. Bhol, S. Swarnalata, S. Manav, S.J. Neena, H. Gopalkrishna, K.S. Akshaya, Femtomolar detection of thiram via sers using silver nanocubes as an efficient substrate, Environ. Sci.: Nano 7 (2020) 3999–4009, https://doi.org/10.1039/D0EN01049A.

[21] Y. Li, et al., Study on annealed graphene oxide nano-sheets for improving the surface enhanced fluorescence of silver nanoparticles, Opt. Laser Technol. 160 (2023), 109054, https://doi.org/10.1016/j.optlastec.2022.109054.

[22] L. Yang, D. Zhang, M. Wang, Y. Yang, Effects of solvent polarity on the novel excited-state intramolecular thiol proton transfer and photophysical property compared with the oxygen proton transfer, Spectrochim. Acta Part A 293 (2023), 122475, https://doi.org/10.1016/j.saa.2023.122475.

[23] T. Ming, H.J. Chen, R.B. Jiang, Q. Li, J.F. Wang, Plasmon controlled fluorescence: beyond the intensity enhancement, J. Phys. Chem. Lett. 3 (2012) 191–202, https://doi.org/10.1021/jz201392k.

[24] W. Wei, Y. Du, L. Zhang, Y. Yang, Y. Gao, Improving SERS hot spots for on-site pesticide detection by combining silver nanoparticles with nanowires, J. Mater. Chem. C 6 (2018) 8793–8803, https://doi.org/10.1039/C8TC01741G.

[25] Q.D. Mai, H.A. Nguyen, T.L.H. Phung, N.X. Dinh, Q.H. Tran, T.Q. Doan, A.T. Le, Silver nanoparticles-based SERS platform towards detecting chloramphenicol and amoxicillin: an experimental insight into the role of HOMO–LUMO energy levels of the analyte in the SERS signal and charge transfer process, J. Phys. Chem. C 126 (17) (2022) 7778–7790, https://doi.org/10.1021/acs.jpcc.2c01818.

[26] Y. Li, Z. Hao, H. Cao, S. Wei, T. Jiao, M. Wang, Study on annealed graphene oxide nano-sheets for improving the surface enhanced fluorescence of silver nanoparticles, Opt. Laser Technol. 160 (2023), 109054, https://doi.org/10.1016/j.optlastec.2022.109054.

[27] Q.H. Zhang, Small and sharp triangular silver nanoplates synthesized utilizing tiny triangular nuclei and their excellent sers activity for selective detection of thiram residue in soil, ACS Appl. Mater. Interfaces 9 (20) (2017) 17387–17398, https://doi.org/10.1021/acsami.7b04365.

[28] S. Zou, L. Ma, J. Li, Y. Liu, D. Zhao, Z. Zhang, Ag nanorods-based surface-enhanced raman scattering: synthesis, quantitative analysis strategies, and applications, Front. Chem. 7 (2019) 376, https://doi.org/10.3389/fchem.2019.0037.

[29] G. Kumar, R.K. Soni, Silver nanocube- and nanowire-based sers substrates for ultra-low detection of PATP and Thiram molecules, Plasmon 15 (2020) 1577–1589, https://doi.org/10.1007/s11468-020-01172-0.

[30] M.K. Francis, B.K. Sahu, P.B. Bhargav, N.A. B.C, A. Das, S. Dhara, Ag nanowires-based SERS substrates with very high enhancement factor, Phys. E 137 (2022) 115080–115086, https://doi.org/10.1016/j.physe.2021.115080.

[31] X.H. Vu, N.D. Dien, T.T.H. Pham, T.T. Trang, N.X. Ca, P.T. Tho, N.D. Vinhc, P. V. Do, The sensitive detection of methylene blue using silver nanodecahedra prepared through a photochemical route, RSC Adv. 10 (2020) 38974–38988, https://doi.org/10.1039/D0RA07869G.

[32] Q. Wang, X. Bai, Y. Zhang, Z. Zhou, M. Guo, J. Zhang, C. Li, C. Wang, S. Chen, Layered assembly of silver nanocubes/polyelectrolyte/gold film as an efficient substrate for surface-enhanced raman scattering, ACS Appl. Nano Mater. 3 (2020) 1934–1941, https://doi.org/10.1021/acsanm.9b02579.

[33] M. Rycenga, X. Xia, C.H. Moran, F. Zhou, D. Qin, Z.Y. Li, Y. Xia, Generation of hot spots with silver nanocubes for single-molecule detection by surface-enhanced Raman scattering, Angew. Chem. Int. Ed. 50 (2011) 5473–5477, https://doi.org/10.1002/anie.201101632.

[34] R. Ambroziak, J. Krajczewski, M. Pisarek, A. Kudelski, Immobilization of cubic silver plasmonic nanoparticles on TiO2 nanotubes, reducing the coffee ring effect in surface-enhanced raman spectroscopy applications, ACS Omega 5 (23) (2020) 13963–13972, https://doi.org/10.1021/acsomega.0c01356.

[35] Y. Liu, S.H. Wu, X.Y. Du, J.J. Sun, Plasmonic Ag nanocube enhanced SERS biosensor for sensitive detection of oral cancer DNA based on nicking endonuclease signal amplification and heated electrode, Sens. Actuators B 338 (2021) 129854–129863, https://doi.org/10.1016/j.snb.2021.129854.

[36] C. Zhu, X. Hu, X. Wang, Silver nanocubes/graphene oxide hybrid film on a hydrophobic surface for effective molecule concentration and sensitive SERS detection, Appl. Surf. Sci. 470 (2019) 423–429, https://doi.org/10.1016/j.apsusc.2018.11.169.

[37] B. Wang, L. Zhang, X. Zhou, Synthesis of silver nanocubes as a SERS substrate for the determination of pesticide paraoxon and thiram, Spectrochim. Acta Part A 121 (2014) 63–69, https://doi.org/10.1016/j.saa.2013.10.013.

[38] S. Ben Jaber, W.J. Peveler, R. Quesada-Cabrera, C.W.O. Sol, I. Papakonstantinou, I. P. Parkin, Sensitive and specific detection of explosives in solution and vapour by surface-enhanced Raman spectroscopy on silver nanocubes, Nanoscale 9 (2017) 16459–16466, https://doi.org/10.1039/C7NR05057G.

[39] L. Liu, Y. Wu, N. Yin, H. Zhang, Hui Ma, Silver nanocubes with high SERS performance, J. Quant. Spectrosc. Radiat. Transfer 240 (2020), 106682, https://doi.org/10.1016/j.jqsrt.2019.106682.

[40] J. Wang, C. Qiu, X. Mu, H. Pang, X. Chen, D. Liu, Ultrasensitive SERS detection of rhodamine 6G and p-nitrophenol based on electrochemically roughened nano-Au film, Talanta 210 (2020), 120631, https://doi.org/10.1016/j.talanta.2019.120631.

[41] W. Fan, M. Yue-E, X. Ling, T. Liu, Free-standing silver nanocube/graphene oxide hybrid paper for surface-enhanced Raman scattering, Chin. J. Chem. 34 (2016) 73–81, https://doi.org/10.1002/cjoc.201500585.

[42] M.L. Mekonnen, C.H. Chen, M. Osada, W.N. Su, B.J. Hwang, Dielectric nanosheet modified plasmonic-paper as highly sensitive and stable SERS substrate and its application for pesticides detection, Spectrochim. Acta Part A (2020) 117484–117493, https://doi.org/10.1016/j.saa.2019.117484.

[43] X. Xiu, Y. Guo, C. Li, Z. Li, D. Li, C. Zang, S. Jiang, A. Liu, B. Man, C. Zhang, High-performance 3D flexible SERS substrate based on graphene oxide/silver nanoparticles/pyramid PMMA, Opt. Mater. Express 8 (2018) 844–857, https://doi.org/10.1364/OME.8.000844.

[44] Q. Zhang, W. Li, L.P. Wen, J. Chen, Y. Xia, Facile synthesis of Ag nanocubes of 30 to 70 nm in edge length with CF_3COOAg as a precursor, Chemistry 16 (33) (2010) 10234–10243, https://doi.org/10.1002/chem.201000341.

[45] S.H. Im, Y.T. Lee, B. Wiley, Y. Xia, Large-scale synthesis of silver nanocubes: the role of HCl in promoting cube perfection and monodispersity, Angew. Chem. Int. Ed Engl. 44 (14) (2005) 2154–2161, https://doi.org/10.1002/anie.200462208.

[46] Y. Sun, Y. Xia, Shape-controlled synthesis of gold and silver nanoparticles, Science 298 (2002) 2176–2179, https://doi.org/10.1126/science.1077229.

[47] P.K. Sahoo, S.S.K. Kamal, T.J. Kumar, B. Sreedhar, A.K. Singh, S.K. Srivastava, Synthesis of silver nanoparticles using facile wet chemical route, Def. Sci. J. 59 (4) (2009) 447–455, https://doi.org/10.14429/dsj.59.1545.

[48] S. Sarkar, R. Das, PVP capped silver nanocubes assisted removal of glyphosate from water—a photoluminescence study, J. Hazard. Mater. 339 (2017) 54–62, https://doi.org/10.1016/j.jhazmat.2017.06.014.

[49] D. Debnath, C. Kim, S.H. Kim, K.E. Geckeler, Solid-state synthesis of silver nanoparticles at room temperature: poly(vinylpyrrolidone) as a Tool, Macromol. Rapid Commun. 31 (2010) 549–553, https://doi.org/10.1002/marc.200900656.

[50] O. Pawar, N.A. Deshpande, S. Dagade, S. Waghmode, P.N. Joshi, Green synthesis of silver nanoparticles from purple acid phosphatase apoenzyme isolated from a new source Limonia acidissima, J. Exp. Nanosci. 11 (1) (2015) 28–37, https://doi.org/10.1080/17458080.2015.1025300.

[51] J. Ou, Y. Hu, L. Huang, et al., pH-sensitive nanocarriers for *Ganoderma applanatum* polysaccharide release via host–guest interactions, J. Mater. Sci. 53 (2018) 7963–7975, https://doi.org/10.1007/s10853-018-2091-0.

[52] M. Majoube, M. Henry, Fourier transform Raman and infrared and surface-enhanced Raman spectra for rhodamine 6G, Spectrochim. Acta Part A: Mol. Spectrosc. 47 (9–10) (1991) 1459–1466, https://doi.org/10.1016/0584-8539(91)80237-D.

[53] Y. Lu, X. Yan, An imprinted organic-inorganic hybrid sorbent for selective separation of cadmium from aqueous solution, Anal. Chem. 76 (2004) 453–457, https://doi.org/10.1021/ac0347718.

[54] T.M. Rodrigues, L.A.H. Kavashima, E.G.M. Adas, B. Antoniassi, M.R.M. Chaves, Adsorption of rhodamine B from aqueous effluents on graphite from spent lithium-ion battery anode, Int. J. Res. Eng. Sci. 4 (9) (2016) 27–36.

[55] C. Wu, E. Chen, J. Wei, Surface enhanced Raman spectroscopy of Rhodamine 6G on agglomerates of different-sized silver truncated nanotriangles, Colloids Surf. A 506 (2016) 450–456, https://doi.org/10.1016/j.colsurfa.2016.07.020.

[56] X.N. He, et al., Surface-enhanced Raman spectroscopy using gold-coated horizontally aligned carbon nanotubes, Nanotechnology 23 (2012) 205702, https://doi.org/10.1088/0957-4484/23/20/205702.

[57] A. de Barros, F.M. Shimizu, C. Santos de Oliveira, F.A. Sigoli, D. Pereira dos Santos, I.O. Mazali, Dynamic behavior of surface-enhanced Raman spectra for rhodamine 6G interacting with gold nanorods: implication for analyses under wet versus dry conditions, ACS Appl. Nano Mater. 3 (8) (2020) 8138–8147, https://doi.org/10.1021/acsanm.0c01530.

[58] S. Yamamoto, H. Watarai, Surface-enhanced Raman spectroscopy of dodecanethiol-bound silver nanoparticles at the liquid/liquid interface, Langmuir 22 (15) (2006) 6562–6569, https://doi.org/10.1021/la0603119.

[59] Y. Zhao, Y. Xie, Z. Bao, Y.H. Tsang, L. Xie, Y. Chai, Enhanced SERS stability of R6G molecules with monolayer graphene, J. Phys. Chem. C 118 (22) (2014) 11827–11832, https://doi.org/10.1021/jp503487a.

[60] J. Ju, W. Liu, C.M. Perlaki, et al., Sustained and Cost-Effective silver substrate for surface enhanced Raman spectroscopy based biosensing, Sci. Rep. 7 (2017) 6917, https://doi.org/10.1038/s41598-017-07186-9.

[61] G. McNy, D. Eustace, W.E. Smith, K. Faulds, D. Graham, Surface-enhanced Raman scattering (SERS) and surface-enhanced resonace Raman scattering (SERRS): a review of applications, Appl. Spectrosc. 65 (2011) 825–837, https://doi.org/10.1366/11-06365.

[62] K. Chiranjeevi, et al., Flow-based approach for scalable fabrication of Ag nanostructured substrate as a platform for surface-enhanced Raman scattering, Chem. Eng. J. 470 (2023), 144019, https://doi.org/10.1016/j.cej.2023.144019.

[63] COMSOL AB, Stockholm, in: COMSOL Multiphysics® (Ed.), Sweden. It is the soft for Numerical Analysis 6 (0).

[64] P.B. Johnson, R.W. Christy, Optical constants of noble metals, Phys. Rev. B 6 (1972) 4370–4379, https://doi.org/10.1103/PhysRevB.6.4370.

[65] O. Rabin, S.Y. Lee, Surface-enhanced Raman scattering, J. Nanotechnol. (2012) 870378–870390, https://doi.org/10.1155/2012/870378.